Stability Improvement of Perovskite Homojunction by Inhibiting the Diffusion of Doping Defects

Jun Ji, Luyao Yan, Xinxin Wang, Shuxian Du, Benyu Liu, Hao Huang, Shujie Qu, Peng Cui, Yingfeng Li, and Meicheng Li*

Perovskite homojunction can promote the separation and oriented transportation of the photocarriers through the built-in electric field, and weaken the dependence of solar cells on the charge transport layer. Although the perovskite homojunction shows great advantages in improving device efficiency, it retains the inherent poor stability of perovskite materials. Herein, it is found that donor defects (MA$^+$ interstitial, I$^-$ vacancy, etc.) in the n-type layer are prone to compensate the acceptor defects (MA$^+$ vacancy, I$^-$ interstitial, etc.) in the p-type layer. This compensation behavior results from the diffusion of doping defects driven by a concentration gradient, which leads to the weakening of the built-in electric field. Furthermore, phenethylammonium iodide is introduced into the perovskite homojunction to inhibit the defect diffusion, which enhances the stability of the homojunction and the corresponding solar cells. After modification, the efficiency of perovskite homojunction solar cells is improved from 8.60% to 9.60%, and retains 80% (standard ≈30%) of initial efficiency after 1000 h aging.

1. Introduction

Organic–inorganic hybrid perovskite optoelectronic materials have been broadly applied in perovskite solar cells (PSCs) as the absorber, due to its long carrier lifetime and high absorption coefficient.[1–6] In the popular PSCs structure, the electron transport layer (ETL) and/or hole transport layer (HTL) play a key role on the efficient photocarrier separation and extraction.[7–11] However, the existence of ETL and HTL will complicate the device structure and limit its application in large-area modules and flexible devices. Recently, the bipolar transport and self-doping characteristics of perovskite materials have attracted more attention. Based on this unique property, the perovskite homojunction (PHJ) was designed and constructed, which could bring a built-in filed and realize the carrier separation without relying on ETL and HTL.[12–15] The reported PHJ shows excellent research value and application potential in device structure simplification and efficiency improvement.

PHJ has received extensive research since it first reported by our group in 2019. We designed and constructed PHJ through defect management, and further assembled it into planar PSCs.[15] The enhancement of carrier separation and device efficiency has been observed, which is proved to be mainly derived from the built-in electric field inside PHJ. This efficiency improvement rooting from the PHJ also confirmed in subsequent reports.[16–19] Sun *et al.* constructed graded bandgap perovskite with intrinsic n–p homojunction, which efficiently boosts carrier separation and finally the efficiency of p–i–n PSC was improved to 21.4%.[16] In addition, perovskite dot homojunction with three layers of CsPbI$_3$ has also been fabricated by Yuan et al., which facilitated the carrier separation and extraction due to the additional driving force of the built-in electric field within PHJ.[18] In the study of PHJ, researchers have reached a consensus that built-in electric field plays a crucial role in device efficiency improvement. However, the poor stability of perovskite materials still exists in the PHJ, which is a serious threat to the maintenance of the built-in electric field.[20,21]

PHJ is constructed of n- and p-type perovskite layers, which can be obtained through self-doping and external doping strategies.[15,22,23] Its stability is threatened by defect concentration gradient on both sides.[24,25] However, as an innovative structure, the stability mechanism of PHJ is still ambiguous, and the main factors leading to the performance degradation of PHJ devices have not been uncovered. Therefore, it is of great significance to study the degradation mechanism of PHJ and develop effective strategies for stability enhancement.

Here, we prepared the PHJ by a combined deposition method, as we reported previously,[15] and research its stability from both material and device perspective. The effective defect in n-type perovskite is called "donor defect," while the effective defect in p-type perovskite is called "acceptor defect." It is found that the donor defects and acceptor defects (referred to as doping defects, including MA$^+$ interstitial, I$^-$ vacancy, MA$^+$ vacancy, I$^-$ interstitial, etc.) on both sides of the PHJ compensate each other through interdiffusion, resulting in the weakening of built-in electric field. Based on this finding, a stability enhancing method through phenethylammonium iodide (PEAI) modification was proposed. Our results provide a technical reference for enhancing the stability of PHJ and related solar cells, which

J. Ji, L. Yan, X. Wang, S. Du, B. Liu, H. Huang, S. Qu, P. Cui, Y. Li, M. Li
State Key Laboratory of Alternate Electrical Power System with Renewable Energy Sources, School of New Energy
North China Electric Power University
Beijing 102206, China
E-mail: mcli@ncepu.edu.cn

is of significance to the further exploration and application of PHJ.

2. Results and Discussion

2.1. Perovskite Homojunction and Device Stability

The perovskite films show n- and p-type conductivity under different growth conditions. Perovskite precursors with excess lead (II) iodide (PbI_2) enlarge the proportion of donor defects in perovskite films obtained by spin coating method, which then crystallized downward and converted into n-type perovskite during thermal annealing. And intrinsic $CH_3NH_3PbI_3$ film was obtained with stoichiometric precursor. Meanwhile, PbI_2 films about 40 nm thick were deposited on glass by thermal evaporation and immersed in methylammonium iodide (MAI) iso-propanol solution to obtain p-type perovskite films. Detailed procedures can be found in the method section. The morphology of three kinds of perovskite films was investigated by scanning electron microscopy (SEM). The surface of n-doped perovskite film is smooth and dense, with large grain size of ≈300 nm, similar to that of intrinsic perovskite film. However, p-doped perovskite film has ≈100 nm fine grain and large surface fluctuation, as shown in **Figure 1**a. Then, to detect the doping property
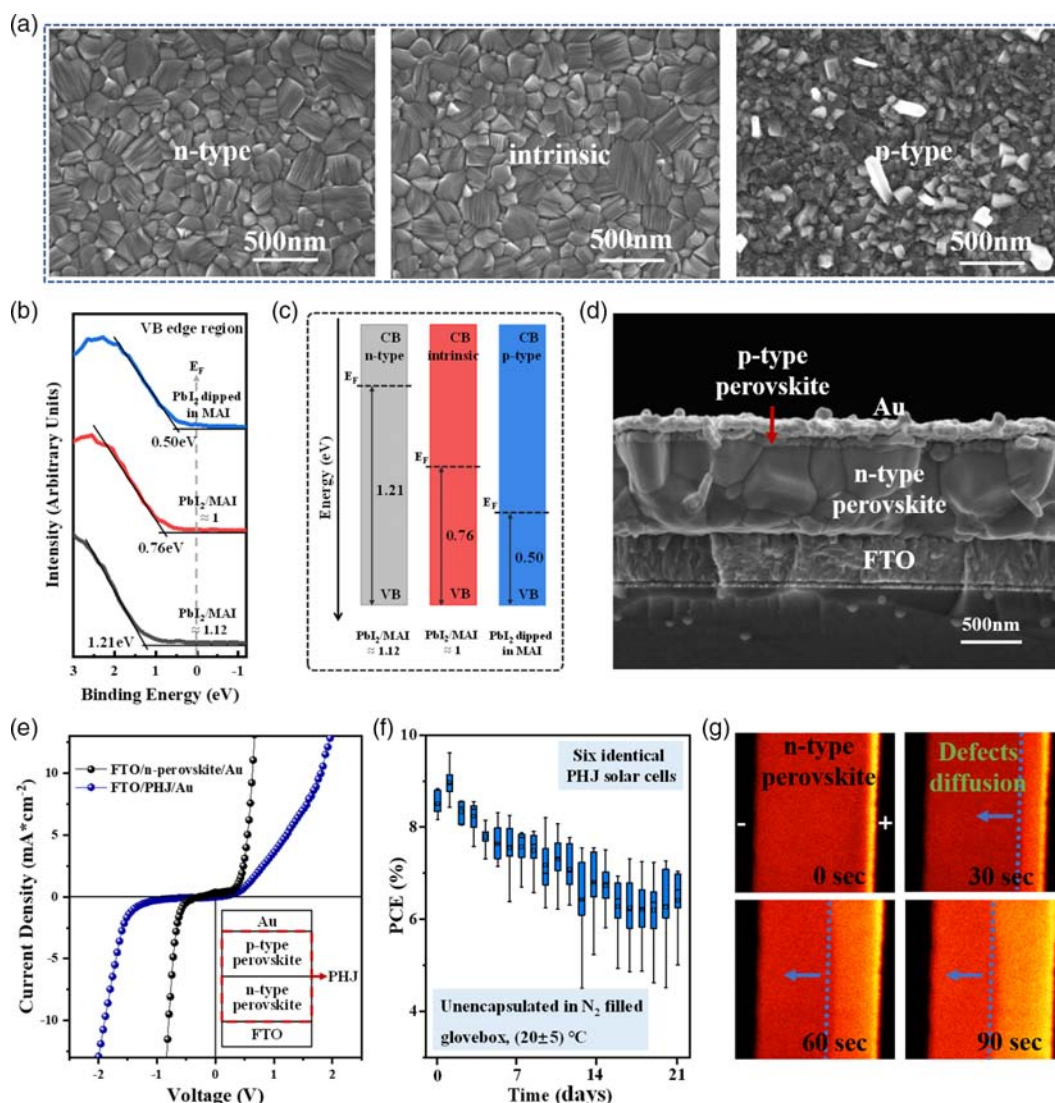

Figure 1. Structure and stability of PHJ. a) Top-view SEM images of the n-type, intrinsic, and p-type perovskite films. b) XPS spectra of the valence band edge region for $MAPbI_3$ films with different molar ratios of PbI_2/MAI. The ratio of 1.12 (black) and 1 (red) indicates the n-type and intrinsic perovskite, whereas the perovskite obtained by dipping PbI_2 in MAI (blue) shows p-type characteristics. c) The energetic levels of the corresponding n-type (gray) and p-type (blue) perovskite films. E_F, CB, and VB represent Fermi level, conductive band, and valence band, respectively. d) A cross-sectional SEM image of PHJ device. The thicknesses of the n-type perovskite, p-type perovskite, and Au electrode are about 700, 60, and 100 nm, respectively. e) J–V character-istics of n-perovskite/electrode Schottky diode and PHJ solar cells under air mass (AM) 1.5 illumination (100 mW cm^{-2}). f) Long-term stability results of six PHJ solar cells in N_2 filled glove box at room temperature. g) Time-dependent PL mapping images of perovskite film under a continuous electric field (10^5 V m^{-1}). The "+" and "−" signs indicate the polarity of the electrodes. The excitation power is 10 mW and the excitation wavelength is 532 nm.

of as-prepared perovskite films, X-ray photoemission spectroscopy (XPS) is carried out on perovskite films. The valence spectra and the schematic energy level of the perovskite films are shown in Figure 1b,c. The energy difference between the valence band and the Fermi level (E_F) is 1.21 eV for the n-type perovskite film with a PbI$_2$/MAI ratio of 1.12 (black), which confirms the n-type doping due to the perovskite's bandgap of 1.55 eV. And the 0.76 eV (red) and 0.5 eV (blue) energy difference verifies the intrinsic (PbI$_2$/MAI $\approx$ 1) and p-type (obtained by dipping PbI$_2$ in MAI) doping characteristics of perovskite films, respectively. Then, we deposited p-type perovskite film on n-type perovskite substrate according to the above method to obtain PHJ. It can be seen from the sectional view that the n-type layer of the PHJ has a thickness of $\approx$700 nm, and the grains run through vertically, which is similar to the intrinsic perovskite layer (Figure S1, Supporting Information). The p-type perovskite layer has a thickness of $\approx$60 nm and the cross-sectional morphology of grains is fine. The boundary between the two layers of perovskite is obvious and shows the morphological characteristics of mutant junction.

The photoelectric characteristics and stability of PHJ were further studied. Perovskite homojunction optoelectronic solar cells were prepared by adding electrodes (FTO and Au) on both sides of the p–n homojunction (Figure 1d). And its current density–voltage (J–V) characteristics are measured by applying a voltage to the top Au contact (Figure 1e, blue line). The PHJ solar cells present J–V characteristics resembling those of a diode because of the large energy barrier for electron injection from n-type perovskite layer to p-type layer, which confirms the strong built-in electric field in the perovskite p–n homojunction. To confirm the effectiveness of the PHJ built-in electric field, Schottky diode with FTO/n-perovskite/Au structure was fabricated and its J–V curve was tested (Figure 1e, black line). It can be seen that Schottky diode J–V curve has smaller threshold voltage and breakdown voltage compared with the PHJ. This indicates that the built-in field of n-perovskite/electrode is much smaller than that of PHJ. At the same time, the photoelectric performance of the PHJ solar cells were characterized, which showed a photoelectric conversion efficiency (PCE) of $\approx$8% (Figure S2, Supporting Information). It is proved that the PHJ devices have photovoltaic effect and can realize photoelectric conversion well. However, the performance of PHJ solar cells is not stable. The PCE was reduced from 8% to 5% after 20 days of storage in a N$_2$-filled glove box at (20 ± 5) °C (Figure 1f). This corresponds to the intrinsic stability of the PHJ solar cells, and has nothing to do with moisture, oxygen, and other external factors. Therefore, the stability of the PHJ solar cells will be measured in nitrogen atmosphere to avoid influence of external factors.

To explore the reason of solar cells degradation, we conducted X-ray diffraction (XRD) characterization of the perovskite films under the same environmental conditions, and found that the n-type perovskite maintained almost the same crystal structure after 10 days aging as the fresh film, without decomposition (Figure S3, Supporting Information). And the surface morphology of p-type perovskite film did not change obviously (Figure S4, Supporting Information). This proves that the performance decay of PHJ solar cells is not caused by material degradation. Furthermore, we observed doping defect migration in the PHJ using confocal photoluminescence (PL) spectrometer. Doping

defect is a kind of electron recombination center, which can cause the quenching of fluorescence. Therefore, the aggregation of doping defects will lead to the attenuation of fluorescence spectrum, and the diffusion process of doping defects in perovskite can be reflected by the change of the attenuation region. We prepared two electrodes on the perovskite film, with a 200 μm slit between the electrodes; the schematic diagram of the setup is shown in Figure S5, Supporting Information. A bias voltage of 20 V was applied between the electrodes, and a confocal PL spectrometer was used to observe the PL mapping spectrum of the slit region (Figure 1g). The dark area boundary in PL Mapping gradually shifts to the negative electrode as time extends, which represents the doping defects with positive charge gradually moves along the bias direction. Diffusion of doping defects may be responsible for the degradation of PHJ solar cell. In order to reveal the degradation mechanism, the effect of doping defects diffusion on the photoelectric performance of the PHJ was further discussed.

2.2. Physical Mechanism of Built-In Electric Field Weakening in Perovskite Homojunction

The conductive doping of perovskite materials is caused by point defects in polycrystalline films. Many kinds of point defects are formed in perovskite polycrystalline films during crystallization, including vacancies, interstitial, cation substitutions, and antisite substitutions (**Figure 2**a). Different defects show different electrical properties due to their unique electronic structures. On the one hand, weak electronegative point defects, such as methylamine interstitial, iodine vacancies, etc., have weak coulomb binding force of outer valence electrons, and valence electrons are easy to leave the point defects and become free electrons in the conduction band. Such point defects are called donor defects. Donor defects make the conduction electron concentration in the system increase, becoming the majority carrier, forming n-type perovskite film.[13] On the other hand, point defects with strong electronegativity, such as iodine interstitial, lead vacancies, etc., can easily obtain valence electrons of covalent bonds of adjacent lattices and become negative centers. The adjacent covalent bond that loses electrons goes on to gain valence electrons from other covalent bonds, creating a moving hole in the valence band. Such point defects become the acceptor defects. Acceptor defects will increase the concentration of holes in the perovskite system and become the majority carrier, forming p-type perovskite layer (Figure 2b). When n-type perovskite and p-type perovskite contact each other, there will be a carrier concentration gradient at the interface. Main carriers in the n-type layer will diffuse to the p-type layer driven by this gradient, leaving positive donor impurities and forming a positive space charge region. Similarly, there will be a negative space charge region in the p-type layer. The potential difference between the positive and negative charge regions causes the electric field (E-field) from the n region to the p region, which is the built-in electric field inside PHJ.

The compensation of doping defects by ion diffusion is the reason for the weakening of the built-in electric field. In the PHJ, n-type layer has a higher concentration of donor defects (MA$^+$ interstitial, I$^-$ vacancy, etc.), while p-type layer has a higher
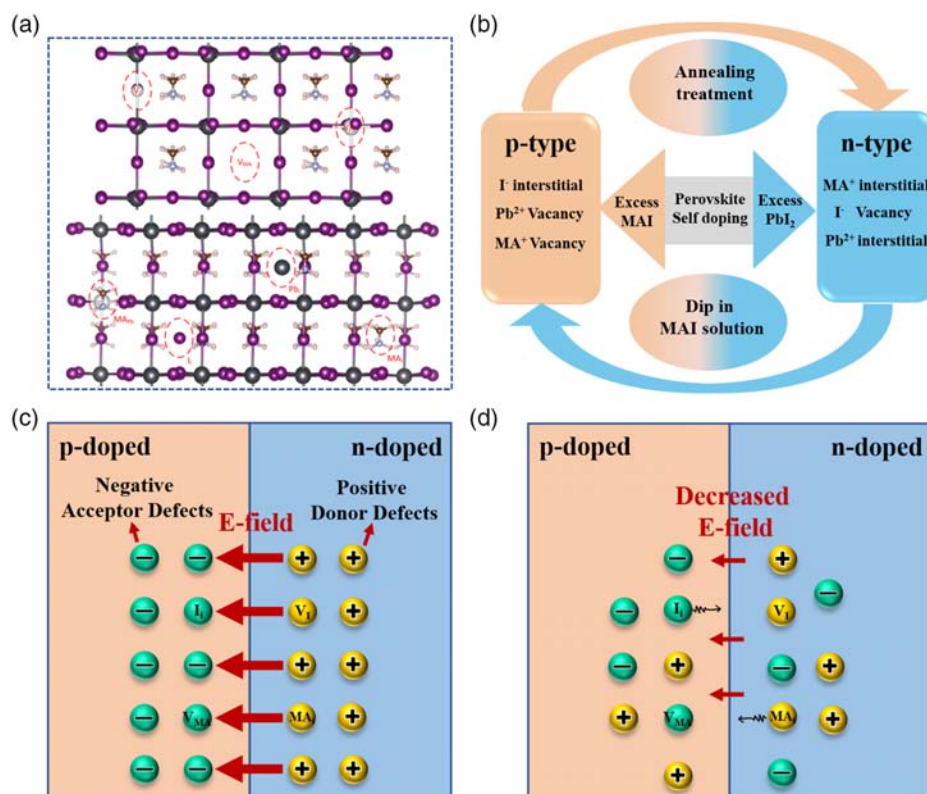
Figure 2. Schematics of PHJ formation and degradation process. a) The schematic defects in MAPbI$_3$. b) Schematic conductivity type conversion of perovskite films by excess MAI or excess PbI$_2$ and possible point defects caused by composition variation. c) Schematic shows how the built-in electric field are formed and degraded at the PHJ.

concentration of acceptor defects (MA$^+$ vacancy, I$^-$ interstitial, etc.), which have low migration energy and easy to diffuse and compensate each other. The diffusion of donor defects from n-type layer to p-type layer driven by concentration gradient will decrease the donor concentration of n-type layer and the acceptor defects in p-type perovskite were compensated. Similarly, the acceptor defects in the p-type layer also diffused to the n-type layer (Figure 2c,d). The diffusion compensation behavior of defects will lead to the decrease of doping concentration on both sides of the homojunction and eventually result in the weakening of the built-in electric field.

The weakening of the built-in electric field is the main factor leading to the degradation of device performance. The photocarriers generated in the perovskite absorbent layer diffuse into the depletion region and drift in a specific direction driven by the built-in electric field. The built-in electric field inside the perovskite layer reduces the recombination rate and promotes the transport of directional carriers.[26,27] In the PHJ solar cell, the built-in electric field is the main driving force of carrier separation, which determines the photoelectric conversion efficiency. It means that the built-in electric field is weakened to failure, which leads to the decline of the photoelectric performance of the devices.

2.3. Enhanced Stability of PHJ Induced by PEAI

PEAI improved the crystal quality of perovskite film. The n-type perovskite films were deposited by incorporation of 0.2–1.2%

(mole ratio) PEAI into precursor. The SEM images of n-type perovskite film with different concentration of PEAI are displayed in **Figure 3**a. Obviously, the grain size increases gradually with the increase of PEAI doping concentration until 0.8%. When the content of PEAI reaches 1.2%, the rupture pores appear in the film. In addition, we characterized the conductive type of PEAI-doped perovskite film. XPS results showed that PEAI-doped film still showed n-type doping and p-type doping (Figure S6, Supporting Information). This is the material basis for the successful preparation of PHJ.

PEAI can effectively inhibit the doping defect diffusion. On the one hand, the benzene group (molecular size ≈0.58 nm) in PEAI can be embedded in the lattice gap of perovskite, blocking the vacancy transition channel of methylamine interstitial. Moreover, iodide ion diffusion through the gap must be coordinated with the rearrangement of methylamine,[28] which greatly reduces the mobility of two main donor defects in n-type perovskites layer. On the other hand, hydrogen atoms of ammonium group in PEAI bonded with perovskite iodine atoms in the form of hydrogen bonds,[29] which strengthened the perovskite lattice, and enlarge the ion diffusion activation energy.

Suppressed doping defects diffusion was observed by confocal laser microfluorescence spectra. In the perovskite film without PEAI doping, an imperceptible bright area boundary in PL mapping gradually shifts to the negative electrode with the extension of time, which represents few donor defects with positive charge have been compensated (Figure 3b). Further, the boundary
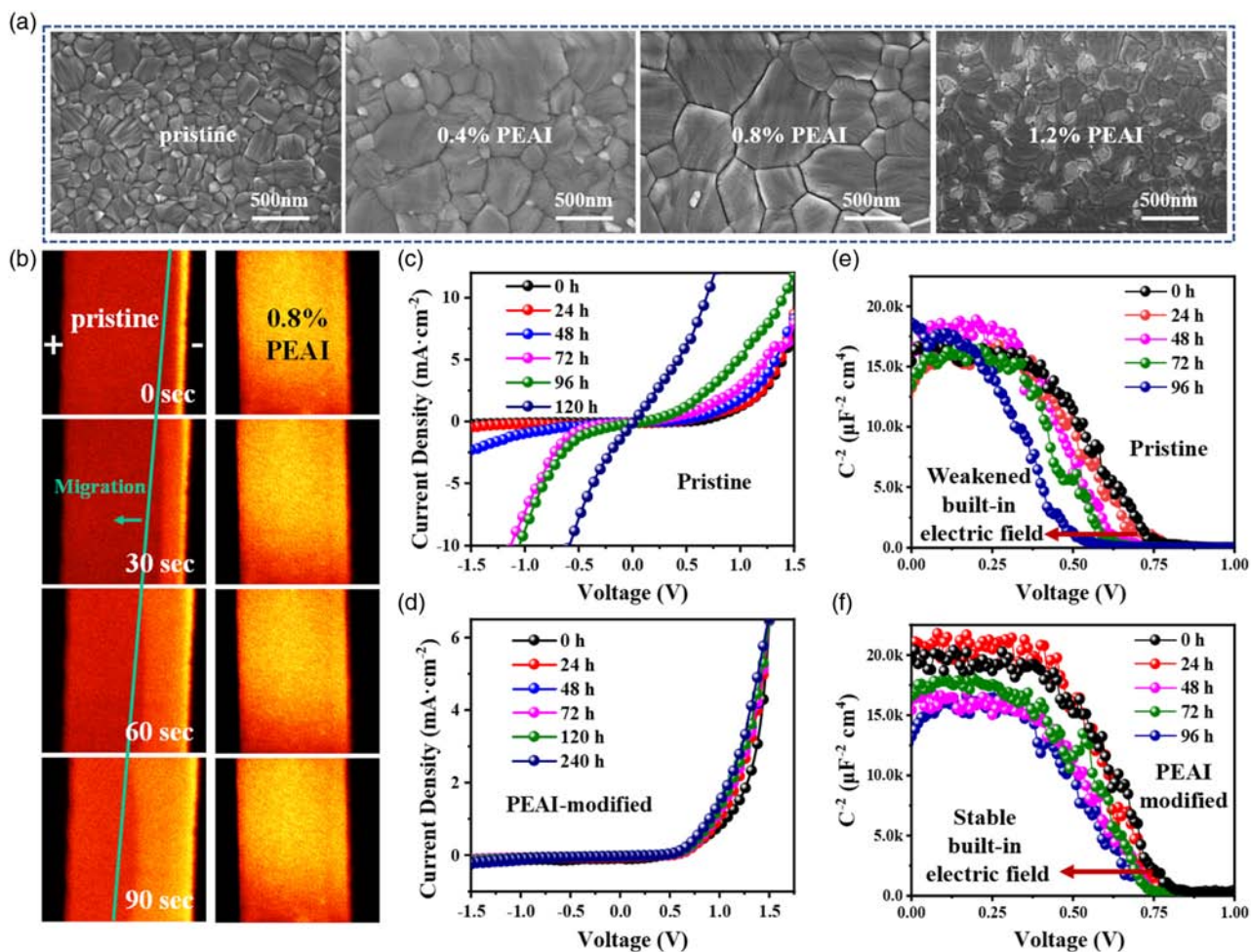
Figure 3. Enhanced stability of PHJ by PEAI. a) Top-view SEM images of perovskite film with and without PEAI modification. b) Time-dependent PL mapping images of PEAI-modified perovskite film. Evolution of *J–V* characteristics over time for c) standard and d) PEAI-modified PHJ. Evolution of built-in electric field identified from the Mott–Schottky curves over time for e) standard and f) PEAI-modified PHJ.

migration of PL mapping did not occur in the perovskite films doped with 0.8% PEAI under the same bias voltage. This result indicates that the donor defects of PEAI-doped perovskite are evenly distributed in the film, and the diffusion of the ion is inhibited. Therefore, 0.8% doping concentration was selected for the following experiments.

PEAI can enhance the stability of the built-in electric field. We store the PHJ in a nitrogen-filled glove box on a heating plate at 85 °C, without exposure to light. The aging process of the built-in electric field inside the PHJ devices with and without PEAI modification was monitored in the form of *J–V* characteristic curves and Mott–Schottky curves. Figure 3c,d shows *J–V* curves of PHJ devices with and without modification, respectively. We conducted forward and reverse scanning of the device within the voltage range from −2 to 2 V, and the results had little deviation (Figure S7, Supporting Information). We found that with the aging time, the diode characteristics of the pristine PHJ devices gradually weakened to disappear, indicating that the built-in electric field gradually weakens under such aging conditions. On the contrary, the diode characteristics of PEAI-modified

PHJ devices almost unchanged, and the built-in electric field remains constant. Figure 3e,f are Mott–Schottky curves of PHJ devices with and without modification respectively. The corresponding *C–V* curves are shown in Figure S8, Supporting Information. We extend the capacitance curve of the depletion layer tangentially, and the intercept with the voltage axis represents the intensity of the built-in electric field.[30] As the aging time increases, the migration of the cutoff points to zero proves that the built-in electric field weakens gradually. For standard solar cells, the built-in field is reduced from 0.75 to 0.5 V. For PEAI-modified solar cells, the built-in field is maintained at 0.8–0.75 V. This indicates that the modification of PEAI can significantly improve the stability of the built-in electric field.

2.4. Enhanced Performance and Stability of PHJ Solar Cells

The modification of PEAI can improve the photoelectric conversion efficiency of PHJ solar cells. We have prepared PHJ solar cells (FTO/n-doped perovskite/p-doped perovskite/

Au) with an area of $0.1 \, cm^2$. Detailed preparation procedures are described in Experimental Section. The photovoltaic performance of the PHJ solar cells with and without PEAI modification was measured under AM1.5G 1 sun illumination in reverse direction. **Figure** 4a exhibits the current–voltage plots of the solar cells with (red) and without (black) PEAI modification. The detailed photovoltaic parameters of short-circuit current density (J_{SC}), open-circuit voltage (V_{OC}), fill factor (FF), and photoelectric conversion efficiency values (PCE) are summarized in inserted table. The best device among the standard PHJ solar cells achieved a PCE of 8.6% with a J_{SC} of $22.12 \, mA \, cm^{-2}$, a V_{OC} of 0.63 V, and an FF of 61.88%. And the PEAI-modified solar cells achieved a PCE of 9.6% with a J_{SC} of $22.38 \, mA \, cm^{-2}$, a V_{OC} of 0.68 V, and an FF of 63.11%. These results indicate that the modification of n-type perovskite by PEAI can significantly improve the PCE of PHJ solar cells. Besides, the stabilized electric power output and the photocurrent density at the maximum power point are measured over a period of 500 s (Figure 4b). By holding a bias near the maximum power output point (+0.43 V), we obtained a stabilized PCE of PEAI-modified solar cells $\approx 9.58\%$, which is similar to the nonstabilized PCE of 9.6% measured for the same cell. And the standard one exhibits a stabilized PCE of $\approx 8.52\%$. The corresponding external quantum efficiency (EQE) measurements show a high photo-to-current conversion over 80% in the range of 400–800 nm, which indicates good utilization of photons in the visible spectrum (Figure 4c). And the integrated current density of 22.18 and $21.72 \, mA \, cm^{-2}$ for standard and PEAI-modified solar cells, respectively, is in good agreement with J–V results. In addition, both solar cells with and without modification show a narrow distribution of PCE with the median value of 8.91% and 7.98% (Figure 4d). And the V_{OC} of PHJ solar cells is distributed between 0.6 and 0.7 V (Figure S9, Supporting Information). These performance results prove a fact that the modification of PEAI greatly improves the performance compared to the standard solar cells, which is consistent with the quality characterization of perovskite film.

The modification of PEAI enhanced the stability of PHJ solar cells. We aged the PHJ solar cells at 85°C in nitrogen filled glove box without light. PEAI-modified PHJ solar cells retained $\approx 75\%$ of their initial PCE after 240 h of aging, whereas standard solar cells retained $\approx 30\%$ (Figure 4e). According to the degradation mechanisms of PHJ during operation described above, fewer PEAI in the n-type perovskite film are beneficial for suppressing doping defects diffusion, which prolongs the operational lifetime of the solar cells. Furthermore, the long-term stability of the PHJ solar cells (stored at room temperature under nitrogen atmosphere without light irradiation) was also tested with the statistical results. This revealed that the PEAI-modified PHJ solar cells only experienced a 20% PCE loss after 1000 h of aging, whereas a PCE loss of up to 67% was found in standard solar cells (Figure 4f). By comparing the thermal stability and room temperature stability, it is proved that high temperature will accelerate the doping defects diffusion in n-type perovskite layer, leading to the weakening of built-in electric field in PHJ, and then result in the degradation of device performance. However, few amounts of PEAI can greatly improve stability of PHJ solar cells by inhibiting defect movement. Therefore, PHJ modified with PEAI has a great potential to be adopted in high-performance devices with enhanced efficiency and lifetime.
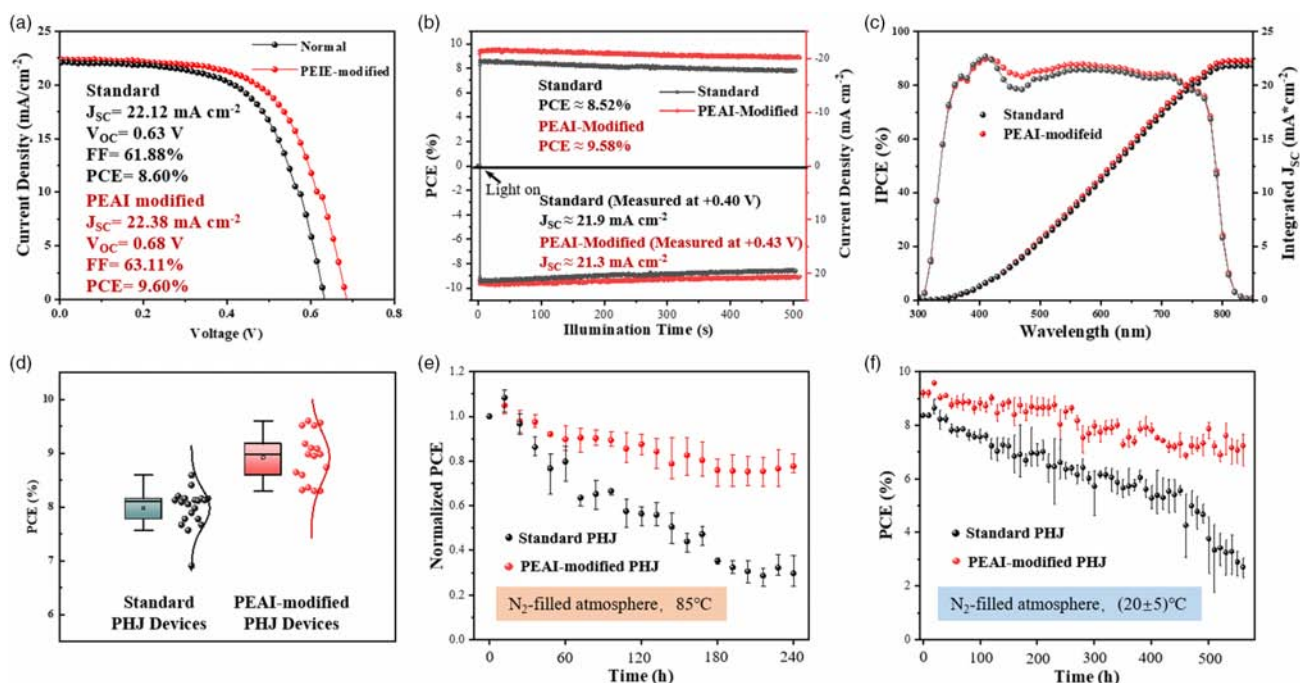

Figure 4. Photovoltaic performance of PHJ solar cells. a) J–V curves, b) the stabilized power output, and c) EQE curves of the champion target PSCs with/without PEAI. d) The efficiency distribution of 20 target PSCs. e) Thermal stability test results of the standard and modified PSCs (5 each) in N_2-filled atmosphere at 85 °C. f) Long-term stability results of the standard and modified PSCs (10 each) in N_2-filled atmosphere at room temperature.

3. Conclusion

In summary, we have studied the stability mechanism of perovskite homojunction and found that the interdiffusion of doping defects in perovskite layer is the main reason for its performance degradation. Donor defects (MA^+ interstitial, I^- vacancy, etc.) in n-type layer are prone to compensate the acceptor defects (MA^+ vacancy, I^- interstitial, etc.) in p-type layer driven by the defect concentration gradient. This compensation behavior will lead to the degradation of built-in electric field and the corresponding solar cells. Fortunately, we found that PEAI can effectively inhibit the diffusion of doping defects, which significantly improves the stability of the perovskite homojunction and related solar cells. The modified perovskite homojunction solar cells retained ≈75% of the initial PCE (standard ≈30%) after 240 h of high-temperature aging at 85 °C. And the long-term storage life exceeds 1000 h. Our results provide a transport-layer-free strategy to prepare efficient and stable perovskite solar cells.

4. Experimental Section

Materials: Methylammonium iodide and 2-phenylethanamine iodide were purchased from Xi'an Polymer Light Technology Corp. (purity: 99.5%). Lead iodide (purity: 99.999%) was purchased from Alfa Aesar. *N,N*-Dimethylformamide (DMF) and dimethyl sulfoxide (DMSO) were purchased from Acros Organics (extra dry).

Fabrication of the Perovskite Homojunction: The perovskite homojunction is constructed with n- and p-type perovskite layers. A one-step spin-coating method was used as to fabricate the n-type perovskite layer in previous published papers [1]. As to the perovskite precursor solution, 159 mg MAI and 517 mg PbI_2 (molar ratio = 1:1.12) were mixed in anhydrous dimethylformamide/dimethylsulphoxide (600 mg/78 mg) solution, which was stirred at room temperature in a glove box. It was spin-coated directly on FTO substrate at 4000 rpm for 25 s. During the spin coating step, 0.5 mL of diethyl ether was poured on the surface at 20 s before the end. The transparent perovskite films were converted into black films by heating at 130 °C for 5 min. For depositing the p-type perovskite film on the n-type film, a new formation method combining evaporating and dipping processes was developed. PbI_2 films with thicknesses of 60 nm were evaporated directly on the surface of n-type perovskite films. Then, these films were dipped in 40 mg mL^{-1} MAI/isopropanol solution. After rinsing with isopropanol, the prepared films were heated at 100 °C for 1 min. Then the perovskite homojunction formed by n- and p-type perovskite films was obtained through the above process. For the PEAI-modified PHJ, 2 mg 2-phenylethanamine iodide (PEAI, CAS:151059-43-7) powder was added in n-type perovskite precursor solution. And then it was spin-coated on top of FTO according to the above method.

PHJ Solar Cell Fabrication: FTO glass substrates were cleaned by dust-free paper first, and then washed with deionized water, ethanol, and acetone twice. Then the FTO substrates were dried by blowing with high-purity nitrogen. After drying in a drying oven at 50 °C for 2 h, the perovskite homojunction was deposited directly on these substrates by the process mentioned above. After that, the Au electrode with a thickness of 100 nm was prepared by the vacuum evaporation equipment. When the electrode thickness is less than 10 nm, the evaporation rate is maintained at 0.1 Å s^{-1}. When the thickness is greater than 10 nm, the evaporation rate is maintained at 0.5 Å s^{-1} until the 100 nm gold electrode is prepared.

Perovskite Film Characterization: The morphologies of the as-prepared $MAPbI_3$ films were characterized by SEM (Hitachi SU8010). The chemical compositions and structures of the perovskite films were analyzed by XRD (Bruker D8 Advance X-ray diffractometer, Cu Kα radiation $\lambda = 0.15406$ nm). The valence spectra were measured by XPS (ESCSLAB 250Xi). All spectra were shifted to account for sample charging

using inorganic carbon at 284.80 eV as a reference. The Mott–Schottky curves of the solar cells were measured by an electrochemical workstation (Zahner Zennium).

PHJ Solar Cell Characterization: Current–voltage curves were measured using a source meter (Keithley 2400) under AM1.5 G irradiation with a power density of 100 mW cm^{-2} from a solar simulator (XES-301S + EL-100). The scanning speed was 2 mV s^{-1}, the scanning range was (−0.1 to 1.2 V), and the test was performed at room temperature (20 ± 5) °C. The step voltage was fixed at 12 mV and the delay time was set at 10 ms. The light intensity was calibrated by a standard silicon cell (the KG-5 mono-Si cell). All of the solar cells had no encapsulation and were tested in ambient air (20 ± 5 °C, ≈40% humidity) and employed a mask with an aperture area of 0.1 cm^2. The EQE was measured using QE-R systems (Enli Tech.). The Mott–Schottky curves of the solar cells were measured by a electrochemical workstation (Zahner Zennium), the disturbed AC voltage was 10 mV, the frequency was 10 KHz, the step width was 0.01 V, and the bias voltage range was −0.5 to 1.2 V. For the PL imaging experiments under electric field, 100 nm thickness of gold was deposited by thermal evaporation through a shadow mask on n-type perovskite films/glass. The electrode distance was 200 μm. The setup used for PL imaging of perovskite films was based on a confocal microscope (Jade mat). The specimen was illuminated by a laser with wavelength of either 532 nm (power = 10 mW), resulting in excitation of free charge carriers.

Supporting Information

Supporting Information is available from the Wiley Online Library or from the author.

Conflict of Interest

The authors declare no conflict of interest.

Data Availability Statement

The data that support the findings of this study are available from the corresponding author upon reasonable request.

[1] A. Kojima, K. Teshima, Y. Shirai, T. Miyasaka, *J. Am. Chem. Soc.* **2009**, *131*, 6050.

[2] L. N. Quan, B. P. Rand, R. H. Friend, S. G. Mhaisalkar, T. W. Lee, E. H. Sargent, *Chem. Rev.* **2019**, *119*, 7444.

[3] N. J. Jeon, J. H. Noh, W. S. Yang, Y. C. Kim, S. Ryu, J. Seo, S. I. Seok, *Nature* **2015**, *517*, 476.

[4] G. Li, J. Wu, J. Song, C. Meng, Z. Song, X. Wang, X. Liu, Y. Yang, D. Wang, Z. Lan, *J. Power Sources* **2021**, *481*, 228857.

[5] S. Wu, Q. Liu, Y. Zheng, R. Li, T. Peng, *J. Power Sources* **2017**, *359*, 303.

[6] Y. Wang, H. Zhang, T. Zhang, W. Shi, M. Kan, J. Chen, Y. Zhao, *Sol. RRL* **2019**, *3*, 1900197.

[7] H. Huang, X. Liu, M. Duan, J. Ji, H. Jiang, B. Liu, S. Sajid, P. Cui, D. Wei, Y. Li, M. Li, *ACS Appl. Energy Mater.* **2020**, *3*, 5039.

[8] H. Min, D. Y. Lee, J. Kim, G. Kim, K. S. Lee, J. Kim, M. J. Paik, Y. K. Kim, K. S. Kim, M. G. Kim, T. J. Shin, S. Il Seok, *Nature* **2021**, *598*, 444.

[9] F. Xie, J. Zhu, Y. Li, D. Shen, A. Abate, M. Wei, *J. Power Sources* **2019**, *415*, 8.

[10] F. Di Giacomo, S. Razza, F. Matteocci, A. D'Epifanio, S. Licoccia, T. M. Brown, A. Di Carlo, *J. Power Sources* **2014**, *251*, 152.

[11] X. Yu, S. Chen, K. Yan, X. Cai, H. Hu, M. Peng, B. Chen, B. Dong, X. Gao, D. Zou, *J. Power Sources* **2016**, *325*, 534.

[12] J. Kim, S. H. Lee, J. H. Lee, K. H. Hong, *J. Phys. Chem. Lett.* **2014**, *5*, 1312.

[13] Q. Wang, Y. Shao, H. Xie, L. Lyu, X. Liu, Y. Gao, J. Huang, *Appl. Phys. Lett.* **2014**, *105*, 163508.

[14] P. Cui, D. Wei, J. Ji, D. Song, Y. Li, X. Liu, J. Huang, T. Wang, J. You, M. Li, *Sol. RRL* **2017**, *1*, 1600027.

[15] P. Cui, D. Wei, J. Ji, H. Huang, E. Jia, S. Dou, T. Wang, W. Wang, M. Li, *Nat. Energy* **2019**, *4*, 150.

[16] H. Sun, K. Deng, J. Xiong, L. Li, *Adv. Energy Mater.* **2020**, *10*, 1903347.

[17] Y. Xiang, Z. Ma, X. Peng, X. Li, B. Chen, Y. Huang, *J. Phys. Chem. C* **2020**, *124*, 20765.

[18] J. Yuan, C. Bi, J. Xi, R. Guo, J. Tian, *J. Phys. Chem. Lett.* **2021**, *12*, 1018.

[19] S. Xiong, Z. Hou, S. Zou, X. Lu, J. Yang, T. Hao, Z. Zhou, J. Xu, Y. Zeng, W. Xiao, W. Dong, D. Li, X. Wang, Z. Hu, L. Sun, Y. Wu, X. Liu, L. Ding, Z. Sun, M. Fahlman, Q. Bao, *Joule* **2021**, *5*, 467.

[20] D. Wei, H. Huang, P. Cui, J. Ji, S. Dou, E. Jia, S. Sajid, M. Cui, L. Chu, Y. Li, B. Jiang, M. Li, *Nanoscale* **2019**, *11*, 1228.

[21] R. Wang, M. Mujahid, Y. Duan, Z. K. Wang, J. Xue, Y. Yang, *Adv. Funct. Mater.* **2019**, *29*, 1808843.

[22] T. Shi, W.-J. Yin, Y. Yan, *J. Phys. Chem. C* **2014**, *118*, 25350.

[23] C. C. Stoumpos, C. D. Malliakas, M. G. Kanatzidis, *Inorg. Chem.* **2013**, *52*, 9019.

[24] D. Wei, F. Ma, R. Wang, S. Dou, P. Cui, H. Huang, J. Ji, E. Jia, X. Jia, S. Sajid, A. M. Elseman, L. Chu, Y. Li, B. Jiang, J. Qiao, Y. Yuan, M. Li, *Adv. Mater.* **2018**, *30*, 1707583.

[25] J. Ji, X. Liu, H. Jiang, M. Duan, B. Liu, H. Huang, D. Wei, Y. Li, M. Li, *iScience* **2020**, *23*, 101013.

[26] L. Meng, S. Wang, F. Cao, W. Tian, R. Long, L. Li, *Angew. Chem., Int. Ed.* **2019**, *58*, 6761.

[27] Q. Zhao, A. Hazarika, X. Chen, S. P. Harvey, B. W. Larson, G. R. Teeter, J. Liu, T. Song, C. Xiao, L. Shaw, M. Zhang, G. Li, M. C. Beard, J. M. Luther, *Nat. Commun.* **2019**, *10*, 2842.

[28] J. L. Minns, P. Zajdel, D. Chernyshov, W. van Beek, M. A. Green, *Nat. Commun.* **2017**, *8*, 15152.

[29] Y. Zheng, Z. Fang, M. Shang, Q. Sun, J. Zheng, Z. Yang, X. Hou, W. Yang, *ACS Energy Lett.* **2021**, *6*, 2328.

[30] O. Almora, C. Aranda, E. Mas-Marzá, G. Garcia-Belmonte, *Appl. Phys. Lett.* **2016**, *109*, 173903.